Convex Programming Energy Management and Components Sizing of A Plug-in Fuel Cell Urban Logistics Vehicle

Xiaohua Wu[a], Xiaosong Hu[b,**], Xiaofeng Yin[a], Lei Li[a], Zhaowei Zeng[a], Volker Pickert[1]

[a]*School of Automobile and Transportation, Xihua University, Chengdu, 610039, China;*
[b]*State Key Laboratory of Mechanical Transmissions, Department of Automotive Engineering, Chongqing University, Chongqing, 400044, China*
[c]*School of Electrical and Electronic Engineering, Newcastle University, UK*

Abstract

This paper devises an optimization framework for efficient energy management and components sizing of a plug-in fuel cell urban logistics vehicle (PFCULV). Based on the structure and system models of the PFCULV, a convex programming (CP) problem is formulated to simultaneously optimize both the control decision and parameters of power sources, including a fuel cell pack and a battery pack. This paper seeks to minimize a summation of energy cost and power sources cost, while satisfying vehicle power demand and battery health requirements. Considering different drive cycles, the optimal parameters and energy costs are systematically investigated. As a result, the optimal battery rated power and energy capacity are not affected by the different drive cycles, given an electric-only range between 40 km and 60 km. Finally, based on the developed CP control law and optimal parameters, we examine the power distribution of the PFCULV in different drive cycles.

Keywords: Plug-in Fuel Cell Vehicle, Urban Logistics Vehicle, Energy Management, Parameters Matching, Convex Programming, Optimization

*This work was supported in part by Science and Technology Department of Sichuan Province (Grant Nos. 2017GZ0104, 2016HH0010), Education Department of Sichuan Province (Grant No. 18ZA0450), Xihua University Fund (Grant No. szjj2018-133).

**Corresponding author (X. Wu and X. Hu equally contributed to this research work.)
Email address: xiaosonghu@ieee.org (Xiaosong Hu)

1. Introduction

1.1. Motivation

With the acceleration of economic development and urbanization, China has put forward higher requirements for energy-saving and emission-reduction performance of urban logistics vehicles (ULVs), an important type of commercial vehicles. Researchers and automobile industries have to develop low-fuel consumption and high-efficiency ULVs. Due to a limited driving range and a long charging time of a battery electric vehicle (EV), growing attention has been paid to fuel cell electric vehicles (FCEVs) [1, 2]. This paper devises an optimization framework for efficient energy management and components sizing of a plug-in fuel cell urban logistics vehicle (PFCULV).

1.2. Literature review

There is a rich literature on FCEVs energy management approaches, which can be generally categorized into sequential quadratic programming (SQP), adaptive control approach, logic threshold control strategy, fuzzy logic control strategy, dynamic programming, predictive control, tracking control, and convex programming (CP).

An SQP based equivalent consumption minimum strategy for a FCEV powered by a fuel cell (FC) system, a battery pack, and a supercapacitor pack is presented in [3], which minimizes its hydrogen consumption and prolongs the FC lifetime. In terms of fuel economy and drivability, the energy management strategy (EMS) of a FC/supercapacitor hybrid electric bus is considered in [4]. Based on the ensemble of well-established methods, high-fidelity vehicle dynamic simulations, and real-world vehicle test data, energy use and air emissions of hydrogen FC electric trucks are provided in [5]. Due to the passive and active EMS, the output characteristics of each power source of a solar cell/FC/battery hybrid unmanned aerial vehicle are investigated in [6]. The EMS of a vehicle powered by an FC system and a Li-ion battery is proposed in [7], based on an

adaptive control approach with fuzzy logic parameter tuning. The impact of FC performance and control strategies on the benefits of hybridization are studied in [8]. The offline strategy (dynamic programming), and online strategy (optimized fuzzy logic controller) for a real FCEV are described in [9]. To coordinate energy sources and power components of a FCEV, an optimal EMS based on specific fuel consumption due to load shifting is defined in [10]. Based on a novel fractional-order extremum seeking method, an online EMS is presented in [11], which can improve both the FC efficiency and durability. An overview of power conditioning system architectures for an FCEV propulsion system, as well as the control strategy to reduce the power losses, is presented in [12]. To minimize hydrogen consumption and simultaneously protect FC health, a two-stage energy management controller (including predictive controller, and tracking controller) is formulated and investigated for a series plug-in FC/Li-ion battery hybrid midsize sedan in [13].

Considering different constraints of maximum velocity and dirving range, components sizes (including the electric machine, power electronics, batteries, etc.,) of an FCEV are optimized in [14], where the impact of the FC size on the vehicle's performance is particularly examined. A logic threshold control strategy and a fuzzy logic control strategy are provided to control a hybrid power supply of an aluminum air FC stack and a supercapacitor pack for a FCEV in [15], where component parameters are analyzed and calculated. Based on a statistical description of driving cycles, energy sources of a FC based collection truck are sized in [16], which shows that a 20 kW FC stack is sufficient for a 13 000 kg collection truck. The impact of different levels of modeling details on the total cost of ownership of a FCEV is investigated through convex optimization in [17], where sizes of its FC system, battery pack, and electric motor are optimized simultaneously. In [18], CP is extended to rapidly and efficiently optimize both the EMS and components (the battery pack and the FC system) sizes for an FC electric bus.

The structure and key parameters for power sources of FCEVs in the available literature are listed in Table 1. The main power source structure is fuel

cell/battery (FC+B), and a few of setups use fuel cell/supercapacitor (FC+S) or fuel cell/battery/supercapacitor (FC+B+S). Most of the existing literature focuses on energy management problems of cars or buses, whereas few are about trucks. Almost all of plug-in (P) batteries are used for cars. However, hydrogen stations are limited, and hydrogen price is expensive at present. The prices of battery and electricity are cheaper than those of FC and hydrogen. Therefore, plug-in fuel cell electric powertrains with relatively large battery sizes could be a more affordable and sustainable solution, particularly for economy-critical truck applications. However, few studies consider optimal component sizes and control strategy (see Table 1, both means sizing and EMS) simultaneously for a plug-in FC/battery truck. The additional plug-in functionality could significantly change parametric optimization and EMS design decisions, versus non-plug-in powertrains. Hence, this paper devises an optimization framework for efficient energy management and components sizing for a PFCULV.

1.3. Contributions

To overcome the downsides of the previous studies, this paper delivers two key contributions to the relevant literature. First, CP is leveraged to optimize both the control decision and parameters of a PFCULV at the same time. To the best knowledge of the authors, this is the first study on the CP-driven joint optimization of control strategy and component sizes for a PFCULV. Considering the PFCULV's electric-only driving distance constraint and the battery lifetime requirement, we optimize the battery energy capacity for the PFCULV. Second, based on different drive cycles and hydrogen prices, we perform a sensitivity study for the power-source parameters and energy cost.

1.4. Outline of paper

The remainder of the paper proceeds as follows. Section 2 details the system structure and models of the PFCULV. The CP problem is formalized in Section 3. The optimization results are discussed in Section 4, followed by conclusions summarized in Section 5.

Table 1: FCEVs literature analysis.

References	Mass kg	Power source strcuture	FC kW	Battery kWh	Other
Ahmadi[19]	1500	FC+B+S	50	7.5	car EMS
Sarioglu[10]	1800	FC+B	70	1.2	car EMS
Xu[20]	2000	FC+B	70	3	car EMS
Martel[21]	1349	FC+B (P)	-	-	car EMS
Geng[13]	1500	FC+B (P)	30	-	car EMS
Song[22]	1600	FC+B (P)	6.5	5.12	car EMS
Fernandez[23]	2290	FC+B (P)	-	16	car EMS
Jensen[14]	1508	FC+B	62.0	17.4	car sizing
Pourabdollah[17]	1600	FC+B (P)	-	-	car sizing
Geng[24]	8000	FC+B (P)	30	-	truck EMS
Ravey[16]	19000	FC+B	20	25	truck sizing
Carignano[4]	13650	FC+S	48	-	bus EMS
Carignano[25]	14100	FC+S	48	-	bus EMS
Hu[18]	134800	FC+B	58	5.6	bus both
Hu[26]	14500	FC+B+S	100	-	bus both

2. Structure and models

2.1. Structure and parameters

We consider the propulsion system of a PFCULV shown in Fig. 1. The ULV is impelled by a traction motor. A DC-DC converter is applied to regulate the FC system current flow into the DC bus, to which a Li-ion battery pack is connected in parallel. The difference between the current demand from the motor inverter and the current flow from the FC system DC-DC converter is offset by the Li-ion battery pack, which can be charged through plugging-in to the grid.

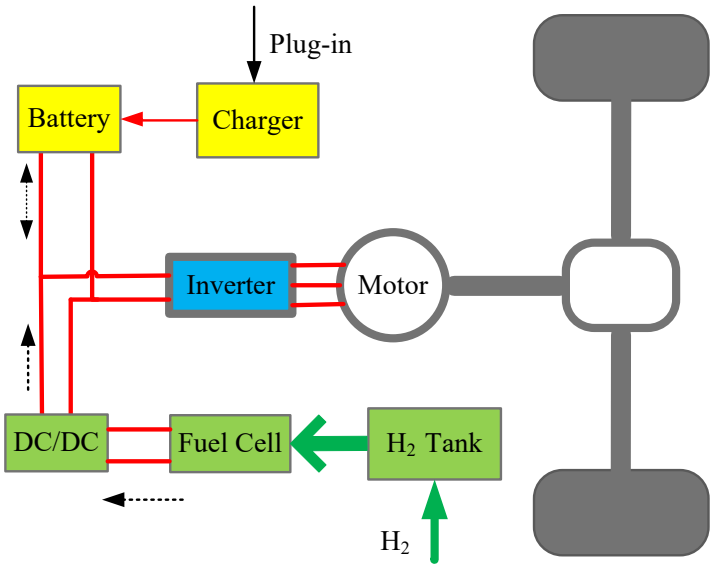

Figure 1: Architecture of the PFCULV propulsion system.

Performance specifications for the PFCULV are listed in Table 2. The key parameters of the PFCULV are listed in Table 3. The parameters of power sources, including the rated power of the FC system, the rated power and energy capacity of the battery pack, need to be matched and optimized.

2.2. FC system modeling

The FC system is the main power source of the PFCULV. The FC system rated power is higher than average driving resistance power (u_a=50 km/h), but lower than the required power when the vehicle is driving at the maximum speed ($u_{\max}$=80 km/h), to avoid a overly large and costly FC system. So, the rated power of the FC system P_{FC} should be satisfied as follows

$$(m_t g f + \frac{C_D A}{21.15} u_a^2) \frac{u_a}{3600 \eta_T} \leq P_{FC} \leq (m_t g f + \frac{C_D A}{21.15} u_{\max}^2) \frac{u_{\max}}{3600 \eta_T}, \quad (1)$$

where m_t is the total mass of the vehicle chasis, the battery, and the FC system. In this paper, the FC system with a power rating of P_{FCb}=50 kW in ADVISOR

Table 2: Performance specifications for the PFCULV.

Specification description	Symbol	Value	Unit
Maximum velocity	$u_{\max}$	$\geq$80	km/h
Average velocity	u_a	50	km/h
0$\sim$50 km/h acceleration time	t_m	$\leq$25	s
Maximum grade	$\alpha_{\max}$	$\geq$20	%
Driving distance of using only hydrogen fuel	d_h	$\geq$200	km
Driving distance of using only the battery with average velocity	d_b	$40\leq d_b \leq 60$	km
Service period	y_t	5	years

(FC-ANL50h2) is considered as the baseline FC system. Its hydrogen consumption is a function of the FC system net power, which is approximated by a quadratic function below [18]:

$$P_h = a_0 P_{fc}^2 + a_1 P_{fc} + a_2, \tag{2}$$

where a_0, a_1, and a_2 are nonnegative power-dependent coefficients. P_h and P_{fc} are the hydrogen power and the net power of the baseline FC system, respectively. The original and approximate hydrogen consumption curves are indicated in Fig. 2.

We assume that the rated power of the FC system targeted in the PFCULV is

$$P_{FC} = P_{FCb} x_{fc}, \tag{3}$$

$$x_{fc,\min} \leq x_{fc} \leq x_{fc,\max}, \tag{4}$$

where x_{fc} is the optimal design parameter of the FC system. $x_{fc,\min}$ and $x_{fc,\max}$ are the minimal and maximal values of x_{fc}, respectively. The hydrogen con-

Table 3: Key parameters of the PFCULV.

Parameter description	Symbol	Value	Unit
Frontal area	A	4.4	m^2
Drag coefficient	C_D	0.75	-
Rolling resistance coefficient	f	0.015	-
Rotation mass conversion factor	δ	1	-
Gross vehicle mass	m_v	6400	kg
Ratio of final drive	i_0	12.9	-
Wheel radius	r	0.367	m
Motor peak power	$P_{m\,\max}$	90	kW
Motor rated power	P_{me}	45	kW
Motor rated speed	n_{me}	1900	rpm
Motor maximum speed	$n_{m\,\max}$	9000	rpm
Efficiency of motor and final drive	η_T	0.9	-
Power of air conditioning	P_{air}	1	kW

sumption of the PFCULV is thus

$$P_{h,k} = a_0 P_{fc,k}^2 + a_1 P_{fc,k} + a_2, \quad k = 0, ..., N-1, \tag{5}$$

where the subscript k is the time index, and N is the final time step of drive cycle. Then, $P_{h,k}$ and $P_{fc,k}$ are the hydrogen power and the net power of the PFCULV FC system, respectively. And $P_{fc,k}$ should respect the following constraint

$$0 \leq P_{fc,k} \leq P_{FC}. \tag{6}$$

2.3. Battery modeling

The battery pack is another power source for the PFCULV. Main principles for battery parameters matching include: (i) it can recover most of the braking energy; (ii) it can work with the FC system to meet the power requirement for

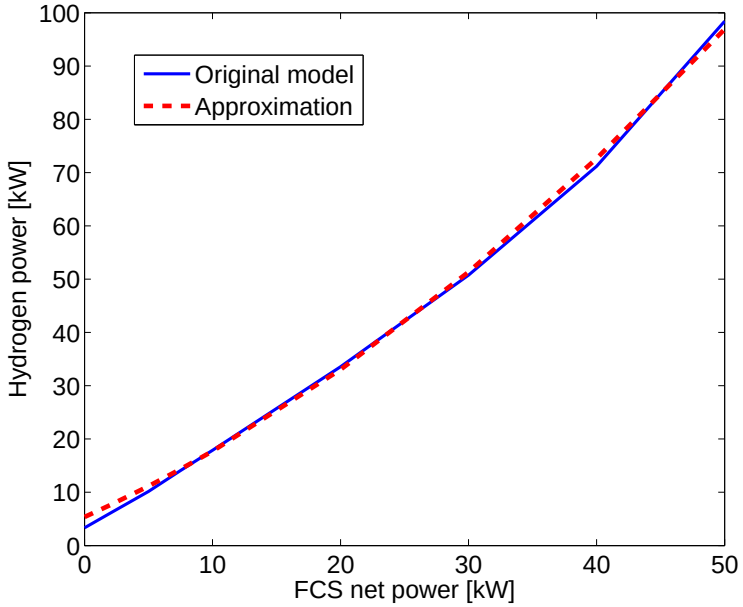

Figure 2: FCS modeling.

vehicle propelling and auxiliary electrical systems in a hybrid mode; (iii) it can meet the requirement for the electric-only driving distance. So, the rated power of the battery pack P_B should be constrained as follows:

$$\frac{P_{me}}{\eta_T} + P_{aux} - P_{FC} \leq P_B \eta_b \leq \frac{P_{me}}{\eta_T}, \tag{7}$$

where P_{me} is the rated power of the motor, and P_{aux} is the power demand of vehicular auxiliary electrical systems. Usually, $P_{aux} = \frac{P_{air}}{0.65}$, with P_{air} being the power for air conditioning [27]. Moreover, η_b is the average battery system efficiency.

To meet the requirement for the electric-only driving distance d_b (40 km $\leq d_b \leq$60 km), the battery energy should constrained by

$$40(\frac{F_t}{3600\eta_T} + \frac{P_{aux}}{u_a}) \leq E_b D_{oD} \eta_b \leq 60(\frac{F_t}{3600\eta_T} + \frac{P_{aux}}{u_a}), \tag{8}$$

where E_b is the battery energy capacity (kWh), D_{oD} is the depth of discharge (%), and F_t is the traction force (N) with an average velocity (u_a=50 km/h),

as calculated by

$$F_t = m_t g f + \frac{C_D A}{21.15} u_a^2. \tag{9}$$

We assume that the battery energy capacity E_b is

$$E_b = \frac{n_0 x_b V_{nom} Q}{3600000}, \tag{10}$$

$$x_{b,\min} \leq x_b \leq x_{b,\max}, \tag{11}$$

where n_0 is the base number of battery cells, x_b is the optimal design parameter of the battery pack, V_{nom} is the nominal voltage of the battery cell, and Q is the battery cell's capacity. Moreover, $x_{b,\min}$ and $x_{b,\max}$ are the minimal and maximal values of x_b, respectively.

The controller also must maintain the battery energy and power within allowable bounds [28, 29],

$$SOC_{\min} E_b \leq E_k \leq SOC_{\max} E_b, \quad k = 0, ..., N, \tag{12}$$

$$-P_B \leq P_{b,k} \leq P_B, \quad k = 0, ..., N-1, \tag{13}$$

where E_k and $P_{b,k}$ are the battery energy and internal power at time k, respectively. The discharge power is assumed to be positive, by convention. $SOC_{\min}$ and $SOC_{\max}$ are the battery's minimal SOC (state of charge) and maximal SOC, respectively. The dynamics of the battery are governed by the following equations:

$$E_{k+1} = E_k + \Delta t P_{b,k}, \quad k = 0, ..., N-1, \tag{14}$$

$$E_0 = E_{init}, \tag{15}$$

$$0 \leq E_0 - E_{end} \leq E_b D_{oD}, \tag{16}$$

$$P_{bloss,k} = (1 - \eta_b)|P_{b,k}|, \quad k = 0, ..., N-1, \tag{17}$$

where Δt is the time interval, and E_{init} and E_{end} are the initial and final battery energy, respectively. Further, $P_{bloss,k}$ is the power loss of the battery system.

Battery degradation always occurs during realistic vehicle operations, and its fading rate depends on a multitude of factors. The energy throughput-based

battery cell state-of-health (SOH) model from [30] is used in this paper, and the derivative of SOH is approximated by a function of the battery cell power $P_{bc,k}$ as follows [31],

$$SOH_{c,k+1} = SOH_{c,k} + \Delta SOH_{c,k}, \quad k = 0, ..., N-1, \tag{18}$$

$$\Delta SOH_{c,k} = \min(b_{j,1} + b_{j,2}|P_{bc,k}|), \quad j = 1, 2, 3, 4, \tag{19}$$

where $b_{j,1}$, $b_{j,2}$ with $j = 1, 2, 3, 4$, are coefficients approximating the SOH derivative, and $SOH_{c,k}$ is the battery cell SOH at time k. The original and approximate battery cell wear models are indicated in Fig. 3. According to the number of battery replacements n_r, the battery cell SOH decrease over a drive cycle is constrained by

$$1 - \Delta SOH_{c,\max} \leq SOH_{c,k} \leq 1, \tag{20}$$

$$SOH_{c,1} - SOH_{c,end} \leq \Delta SOH_{c,\max}, \tag{21}$$

$$\Delta SOH_{c,\max} = \frac{L_d(n_r+1)}{L_a y_t}. \tag{22}$$

where $\Delta SOH_{c,\max}$ is the maximum allowed change in SOH over a drive cycle, y_t is the vehicle service period, L_a is the average distance traveled annually, and L_d is the length of drive cycle. Furthermore, $SOH_{c,1}$ and $SOH_{c,end}$ are the initial and final battery cell SOH values over a drive cycle, respectively.

Since the battery cell has a very flat OCV curve in the allowed SOC window [26], $P_{b,k} \approx \frac{n_0 x_b P_{bc,k}}{1000}$. Using a variable change, $\overline{SOH}_k = n_0 x_b SOH_{c,k}$. Eq. (17) can be rewritten as

$$\Delta\overline{SOH}_k = \min(b_{j,1} n_0 x_b + b_{j,2}|1000 P_{b,k}|), \quad j = 1, 2, 3, 4. \tag{23}$$

Since the maximum allowed change in SOH over a drive cycle $\Delta SOH_{c,\max}$, is very small, an additional variable change is required to scale the SOH within a certain range [0, 1]. Let SOH_k be a new variable [32], such that

$$\overline{SOH}_k = SOH_k n_0 x_{b,\max} \Delta SOH_{c,\max} + n_0 x_b (1 - \Delta SOH_{c,\max}). \tag{24}$$

Differentiate Eq. (24) to get

$$\Delta SOH_k = \frac{\Delta\overline{SOH}_k}{n_0 x_{b,\max} \Delta SOH_{c,\max}}. \tag{25}$$

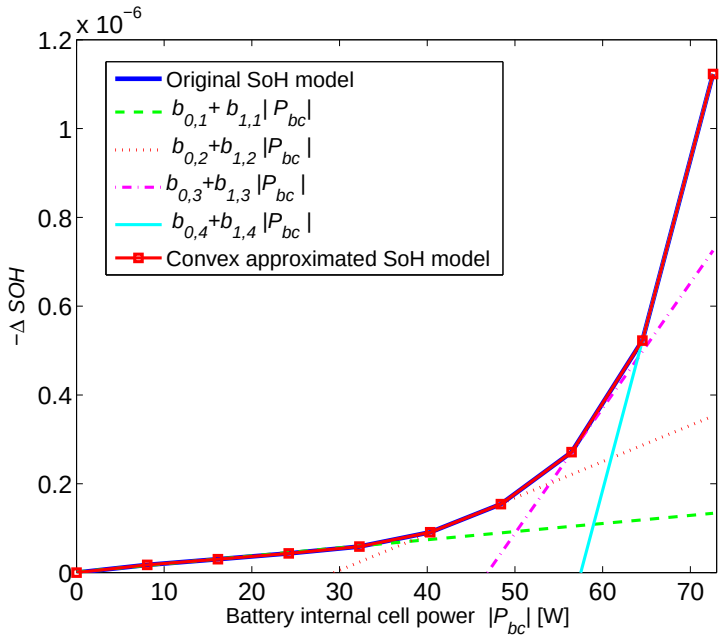

Figure 3: Battery cell wear model[31].

And SOH_k is constrained by

$$\Delta SOH_k = SOH_{k+1} - SOH_k, \tag{26}$$

$$0 \leq SOH_k \leq \frac{x_b}{x_{b,\max}}. \tag{27}$$

2.4. System model

The PFCULV satisfies the dynamic equation of the vehicle during driving, and fully supplies the required energy from the battery and FC systems. The power balance is depicted by

$$P_{b,k} + P_{fc,k} = P_{u,k} + P_{aux} + P_{bloss,k}, \tag{28}$$

where the PFCULV running power demand is expressed as

$$P_{u_k} = (m_t g f + \frac{C_D A}{21.15} u_k^2 + \delta m_t \frac{\Delta u_k}{3.6\Delta t}) \frac{u_k}{3600\eta_T}, \tag{29}$$

where u_k is the velocity of the PFCULV at time k. The toal mass of the chassis, battery, and FC systems can be expressed as

$$m_t = m_v + m_b n_0 x_b + m_{fc} x_{fc}, \tag{30}$$

where m_v, m_b, and m_{fc} are the gross vehicle mass, the battery cell mass, and the baseline FC system mass, respectively.

3. Optimization problem formulation

The convex objective function $F(x)$, which is of great interest to the PFCULV owner, is formulated to minimize a summation of the total energy cost, and the power source cost, for which we mainly consider the costs of the FC system and the battery pack:

$$F = C_{bf} + B_c + F_{cc}, \tag{31}$$

where C_{bf} is the total energy cost over a drive cycle, including both hydrogen and electricity costs, B_c is the battery cost, and F_{cc} is the FC system cost. Costs of the FC system and the battery are first normalized per kilometer (km), and then multiplied with the length of drive cycle.

It is assumed that the payment for the FC system is divided in equal amounts over a period of the PFCULV service period, $y_t = 5$ years, with a $r_y = 5\%$ yearly interest rate. The equivalent FC system cost related to a drive cycle is obtained by multiplying the length L_d with the FC price per km, given the average annual mileage L_a:

$$F_{cc} = c_f P_{FC}(1 + r_y \frac{y_t + 1}{2}) \frac{L_d}{L_a y_t}, \tag{32}$$

where c_f is the FC price per kW.

The battery equivalent cost, B_c, is calculated similarly:

$$B_c = c_b E_b (1 + r_y \frac{1 + \frac{y_t}{n_r + 1}}{2}) \frac{L_d (n_r + 1)}{L_a y_t}, \tag{33}$$

where c_b is the battery price per kWh.

The energy cost C_{bf} includes costs of hydrgen and electricity:

$$C_{bf} = \frac{c_h}{C_h} \sum_{k=0}^{N-1} P_{h,k} + c_e(E_{init} - E_{end}), \tag{34}$$

where c_e is the electricity price, c_h is the hydrogen cost per kg in (yuan), and C_h is the lower heating value of hydrogen in (J/g).

The optimization variables include the state variables E_k, SOH_k, the control variables $P_{fc,k}$, $P_{b,k}$, and the optimal design parameters P_B, x_b, and x_{fc}. It is easy to see that the objective function F is convex with respect to $P_{fc,k}$ and E_k.

According to the FC system model, the FC system constraints are Eqs. (1), (4), and (6), with $m_t = m_v + m_b n_0 x_b + m_{fc} x_{fc}$ and $P_{FC} = P_{FCb} x_{fc}$. It is easy to see that the FC system constraints are linear inequality functions, and thus convex.

According to the battery model, the battery constraints are Eqs. (7), (8), (11)-(16), (25), and (27), with $F_t = m_t gf + \frac{C_D A}{21.15} u_a^2$, $E_b = \frac{n_0 x_b V_{nom} Q}{3600000}$, $\Delta SOH_{c,\max} = \frac{L_d(n_r+1)}{L_a y_t}$, $\Delta \overline{SOH}_k = \min(b_{j,1} n_0 x_b + b_{j,2} |1000 P_{b,k}|)$, and $\Delta SOH_k = SOH_{k+1} - SOH_k$. It is easy to see that Eqs. (7), (8), (11)-(13), (16), and (27) are linear inequality functions, and thus convex. Eqs. (14) and (15) are linear equality functions, and thus ensure convexity. Eq. (25) is an absolute equality function, which are not affine. In a standard convex optimization problem, only affine equality constraints are tolerated. However, relaxing Eq. (25) to an inequality gives a convex problem without qualitatively altering the original problem as follows [33, 34],

$$\Delta SOH_k \leq \min(b_{j,1} n_0 x_b + b_{j,2} |1000 P_{b,k}|)/n_0/x_{b,\max}/\Delta SOH_{c,\max}. \tag{35}$$

According to Eqs. (28)-(30), the PFCULV's power balance constraints can be expressed as

$$P_{b,k} + P_{fc,k} = (m_t gf + \frac{C_D A}{21.15} u_k^2 + \delta m_t \frac{\Delta u_k}{3.6 \Delta t}) \frac{u_k}{3600 \eta_T} + P_{aux} + (1 - \eta_b) |P_{b,k}|. \tag{36}$$

Eq. (36) is an absolute equality function, which is not affine. However, relaxing Eq. (36) to an inequality gives a convex problem without qualitatively altering the original problem as follows [33, 34],

$$P_{b,k} + P_{fc,k} \geq (m_t g f + \frac{C_D A}{21.15} u_k^2 + \delta m_t \frac{\Delta u_k}{3.6 \Delta t}) \frac{u_k}{3600 \eta_T} + P_{aux} + (1 - \eta_b)|P_{b,k}|. \tag{37}$$

The overall convex optimization framework is summarized in Table 4. Thanks to the convexity, a globally optimal solution with arbitrary initialization can be readily accomplished.

Table 4: Convex optimization framework for combined the PFCULV dimensioning and control.

(1)	The driving cycle, vehicle parameters, and key parameters of power sources are firstly specified.
(2)	For $k = 1, ..., N$, do the optimization below Optimization variables: E_k, SOH_k, $P_{fc,k}$, $P_{b,k}$, P_B, x_b, x_{fc}. Expressions: m_t, P_{FC}, $P_{h,k}$, F_t, E_b, ΔSOH_k, C_{bf}, B_c, F_{cc}. Objective function: Eq. (31). Inequality constraints: Eqs. (1), (4), (6)-(8), (11)-(13), (16), (27), (35), (37). Equality constraints: Eqs. (14), (15).

4. Results & discussion

This section analyses the properties of the proposed CP approach. The CVX-tool is employed to parse the optimization problem. All the simulations are run on a PC with a 2.50 GHz Intel Core i5-6300u CPU and 8 GB of internal memory. Thanks to the mentioned advantages of the proposed method, the optimal components size and control strategy are simultaneously obtained in the Matlab environment. The basic parameters of the FC system, and the battery utilized in the optimization for the PFCULV are listed in Table 5.

Table 5: Key parameters of power sources for the PFCULV.

Specification description	Symbol	Value	Unit
Hydrogen lower heating value	C_h	120000	J/g
Baseline FC system rated power	P_{FCb}	50	kW
Baseline FC system mass	m_{fc}	223.38	kg
Nominal capacity	Q	8280	As
Nominal voltage	V_{nom}	3.3	V
Battery cell mass	m_c	0.07	kg
Deepth of dicharge	D_{oD}	0.7	-
Average battery efficiency	η_b	0.92	-
Maximum SOC	$SOC_{\max}$	0.9	-
Minimum SOC	$SOC_{\min}$	0.2	-
Initial SOC	SOC_{init}	0.9	-
Base number of battery cells	n_0	3000	-
Minimum x_b	$x_{b,\min}$	0.01	-
Maximum x_b	$x_{b,\max}$	2	-
Minimum x_{fc}	$x_{fc,\min}$	0.1	-
Maximum x_{fc}	$x_{fc,\max}$	2	-
Number of battery replacements	n_r	1	-

4.1. Parameters optimization of power sources

Referring to the Bloomberg New Energy Finance (BNEF) survey, the average price of a Li-ion battery pack might vary from 680 yuan/kWh(100 $/kWh) to 1421 yuan/kWh (209 $/kWh) in 2025 [35, 36]. In light of the report of US Department of Energy, hydrogen fuel cell per kW varies from 204 yuan (30 $) to 6800 yuan (1000 $) [37]. In China, the electricity price for EVs is about 1 yuan/kWh, and the hydrogen price is 40 yuan/kg at present. In Chengdu, if hydrogen is produced by distributed energy, such as hydropower, its price will be about 15 yuan/kg. If the battery pack price is 1000 yuan/kWh,

the FC price is 10000 yuan/kW, the electricity price is 1 yuan/kWh, and the hydrogen price is 40 yuan/kg, the optimal values of the battery and the FC systems for four drive cycles are shown in Table 6. The four drive cycles include, (i) the WVUSUB drive cycle represents typical suburban driving for a heavy vehicle; (ii) the CSHVR drive cycle represents typical city-suburban driving for a heavy vehicle; (iii) the WVUCITY drive cycle represents typical city driving for a heavy vehicle; (iv) the CBDTRUCK drive cycle represents central business district test cycle for trucks. For the four drive cycles, the optimal battery rated power maintains constant, equaling to 54.35 kW. The reason for this result may be a cheap price of the battery and the constraint $P_B\eta_b \leq \frac{P_{me}}{\eta_T}$. And the optimal battery energy capacity is approximately 29 kWh. This is due to the PFCULV's constraint that the electric-only driving distance with an average velocity (50 km/h) is more than 40 km, but less than 60 km. It is easily observed that varying drive cycles only affect the size of the FC system.

Table 6: Optimal results of the FC system rated power, battery rated power, and energy capacity for the PFCULV in different drive cycles.

Drive cycles	P_{FC}	P_B	E_b	$V_{\max}$	L_a	$acc_{\max}$
	kW	kW	kWh	km/h	km	m/s^2
WVUSUB	44.81	54.35	29.06	72.10	11.97	1.29
CSHVR	36.59	54.35	28.96	70.49	10.81	1.16
WVUCITY	30.07	54.35	28.87	57.65	5.32	1.14
CBDTRUCK	21.62	54.35	28.76	32.19	3.51	0.36

4.2. Sensitivity to parameters of FC system

In this subsection, we account for a simple but nontrivially useful sensitivity analysis to parameters of the FC system for the PFCULV, where sub-optimal parameters of the FC system are contrasted to the optimal parameters of CP. Given sub-optimal parameters of the FC system meeting necessary design requirements (Eqs. (1), (4), and (6)), and E_b=29 kWh, P_B = 54.35 kW, c_e=1

yuan/kWh, and c_h=40 yuan/kg, the control results of CP for different drive cycles are shown in Table 7. In the table, C_T, C_e, and C_h are the total energy cost, electricity cost, and hydrogen cost, respectively. Since the hydrogen price is more expensive than the electricity price, and the length of drive cycle is less than 40 km, electricity is the main energy for the vehicle propulsion. Inceasing the FC rated power leads to increased hydrogen consumption. For example, in the WVUCITY cycle, when the FC rated power is 50 kW, the total cost increase is up to 61.08%.

4.3. Energy cost based on different hydrogen prices and drive cycle lengths

This subsection presents the PFCULV energy cost in concatenated CSHVR drive cycles with different prices of hydrogen. The single CSHVR drive cycle and vehicle power demand are described in Fig. 4, which represents typical city-suburban driving for a heavy vehicle, and is suitable for ULV. Based on optimal results of the battery energy capacity E_b=28.96 kWh, the rated power P_B = 54.35 kW, and the FC system rated power P_{FC}=36.59 kW, the total energy cost, electric cost, and hydrogen cost for different numbers of CSHVR drive cycles are shown in Table 8. Two different hydrogen prices, including 40 yuan/kg and 15 yuan/kg are considered. When hydrogen is the main energy of the PFCULV in a long trip, the price change of hydrogen will significantly affect the fuel economy of the PFCULV. If the hydrogen price is 40 yuan/kg, when the number of CSHVR drive cycle is not more than 5, electricity is the main energy, and the total energy cost per km is about 0.73 yuan. When the number of CSHVR drive cycle is more than 5, the electricity cost is constant, equal to 20.18 yuan. However, if the hydrogen price is 15 yuan/kg, hydrogen is the main energy, and the total energy cost per km is about 0.35 yuan, and the electricity cost is always zero. The energy cost decrease is approximately 52.05% less for the c_h=15 yuan/kWh case, relative to the c_h=40 yuan/kWh case.

4.4. Example of energy management strategy

Based on the optimal results of the battery energy capacity E_b=28.96 kWh, the rated power P_B = 54.35 kW, the FC system rated power P_{FC}=36.59 kW, the

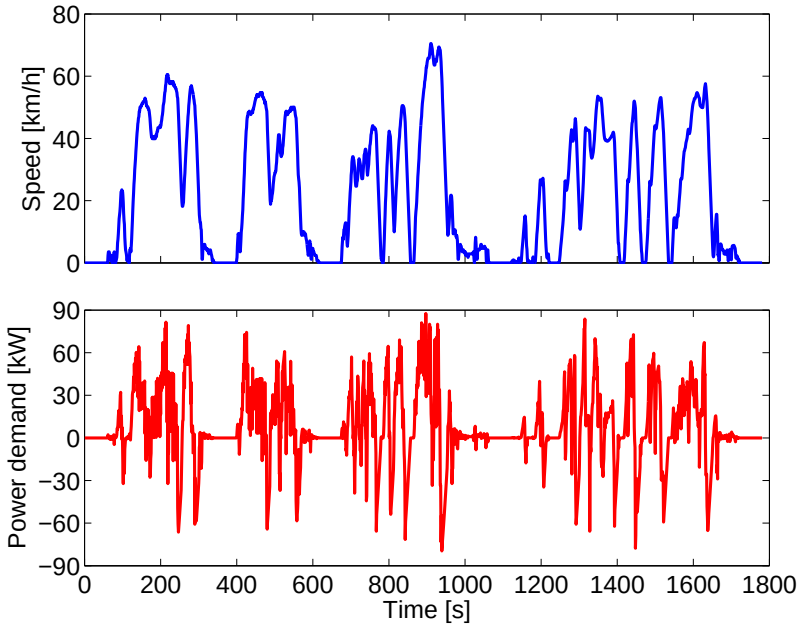

Figure 4: Speed and power demand for a single CSHVR drive cycle.

electricity price c_e=1 yuan/kWh, and two different hydrogen prices, including 40 yuan/kg and 15 yuan/kg, this subsection presents the CP control law for the PFCULV with different lengths of drive cycles.

The optimal power allocations over a single CSHVR drive cycle and 5 concatenated CSHVR drive cycles are described in Fig. 5, including the battery power and the FC system power. According to Fig. 5-(b), every cycle's power allocation is almost the same in the 5 CSHVR drive cycles.

The battery SOC trajectories are shown in Fig. 6. If the hydrogen price is 40 yuan/kg, the battery SOC decreases with the trip distance. If the trip length is larger than the maximum battery-only driving distance, the end of SOC will equal to the mimimum SOC (20%). If the hydrogen price is 15 yuan/kg, the end of battery SOC will equal to the maximum SOC (90%) with a charge sustenance, regardless of driving mileage.

The battery cell power profiles and the associated SOH trajectories for a

single CSHVR drive cycle and 5 CSHVR drive cycles are shown in Fig. 7. For both hydrogen prices, it is evident that the majority of the battery charging occurs during vehicle deceleration, and discharging occurs during vehicle acceleration. The change trend of the battery power is severe and overall similar to the vehicle's power demand. The change trend of the FC system power is relatively gentle, which is always located in high-efficiency regions. When the hydrogen price is 15 yuan/kg, the FC system power is higher than that in the case of 40 yuan/kg, in order to use more hydrogen.

5. Conclusions

This paper develops a CP framework for optimal energy management and component sizing of a PFCULV. The CP problem is mathematically formulated to optimize the power allocation between the FC system and the battery pack. At the same time, the CP strategy explicitly takes into account the optimization of the PFCULV power sources parameters. Different drive cycles and hydrogen prices are also considered in extensive simulation campaigns. Key findings are summarized below:

(1) Based on four different drive cycles, the optimal battery rated power is 54.35 kW, and the optimal battery energy capacity is approximately 29 kWh. The varying drive cycles only affect the size of the FC system.

(2) The price of hydrogen affects the control strategy for the power distribution, which significantly influences the fuel economy of the PFCULV.

The proposed framework can be extended to incorporate thermal dynamics of the battery and FC systems in our future work.

References

[1] H. Chen, Z. Song, X. Zhao, T. Zhang, P. Pei, C. Liang, A review of durability test protocols of the proton exchange membrane fuel cells for vehicle, Applied Energy 224 (2018) 289 – 299.

[2] T. Zhang, P. Wang, H. Chen, P. Pei, A review of automotive proton exchange membrane fuel cell degradation under start-stop operating condition, Applied Energy 223 (2018) 249 – 262.

[3] H. Li, A. Ravey, A. N'Diaye, A. Djerdir, A novel equivalent consumption minimization strategy for hybrid electric vehicle powered by fuel cell, battery and supercapacitor, Journal of Power Sources 395 (2018) 262 – 270.

[4] M. G. Carignano, R. Costa-Castell, V. Roda, N. M. Nigro, S. Junco, D. Feroldi, Energy management strategy for fuel cell-supercapacitor hybrid vehicles based on prediction of energy demand, Journal of Power Sources 360 (2017) 419 – 433.

[5] D. Y. Lee, A. Elgowainy, A. Kotz, R. Vijayagopal, J. Marcinkoski, Life-cycle implications of hydrogen fuel cell electric vehicle technology for medium- and heavy-duty trucks, Journal of Power Sources 393 (2018) 217 – 229.

[6] B. Lee, S. Kwon, P. Park, K. Kim, Active power management system for an unmanned aerial vehicle powered by solar cells, a fuel cell, and batteries, IEEE Transactions on Aerospace and Electronic Systems 50 (4) (2014) 3167 – 3177.

[7] J. Chen, C. Xu, C. Wu, W. Xu, Adaptive fuzzy logic control of fuel-cell-battery hybrid systems for electric vehicles, IEEE Transactions on Industrial Informatics 14 (1) (2018) 292 – 300.

[8] P. Thounthong, V. Chunkag, P. Sethakul, B. Davat, M. Hinaje, Comparative study of fuel-cell vehicle hybridization with battery or supercapacitor storage device, IEEE Transactions on Vehicular Technology 58 (8) (2009) 3892 – 3904.

[9] A. Ravey, B. Blunier, A. Miraoui, Control strategies for fuel-cell-based hybrid electric vehicles: From offline to online and experimental results, IEEE Transactions on Vehicular Technology 61 (6) (2012) 2452 – 2457.

[10] I. L. Sarioglu, O. P. Klein, H. Schroder, F. Kucukay, Energy management for fuel-cell hybrid vehicles based on specific fuel consumption due to load shifting, IEEE Transactions on Intelligent Transportation Systems 13 (4) (2012) 1772 – 1781.

[11] D. Zhou, A. Al-Durra, I. Matraji, A. Ravey, F. Gao, Online energy management strategy of fuel cell hybrid electric vehicles: A fractional-order extremum seeking method, IEEE Transactions on Industrial Electronics 65 (8) (2018) 6787 – 6799.

[12] U. R. Prasanna, P. Xuewei, A. K. Rathore, K. Rajashekara, Propulsion system architecture and power conditioning topologies for fuel cell vehicles, IEEE Transactions on Industry Applications 51 (1) (2015) 640 – 650.

[13] B. Geng, J. K. Mills, D. Sun, Two-stage energy management control of fuel cell plug-in hybrid electric vehicles considering fuel cell longevity, IEEE Transactions on Vehicular Technology 61 (2) (2012) 498 – 508.

[14] H. B. Jensen, E. Schaltz, P. S. Koustrup, S. J. Andreasen, S. K. Kaer, Evaluation of fuel-cell range extender impact on hybrid electrical vehicle performance, IEEE Transactions on Vehicular Technology 62 (1) (2013) 50 – 60.

[15] Y. Zhang, Y. Mou, Z. Yang, An energy management study on hybrid power of electric vehicle based on aluminum air fuel cell, IEEE Transactions on Applied Superconductivity 26 (7) (2016) 1 – 6.

[16] A. Ravey, N. Watrin, B. Blunier, D. Bouquain, A. Miraoui, Energy-source-sizing methodology for hybrid fuel cell vehicles based on statistical description of driving cycles, IEEE Transactions on Vehicular Technology 60 (9) (2011) 4164 – 4174.

[17] M. Pourabdollah, B. Egardt, N. Murgovski, A. Grauers, Convex optimization methods for powertrain sizing of electrified vehicles by using differ-

ent levels of modeling details, IEEE Transactions on Vehicular Technology 67 (3) (2018) 1881 – 1893.

[18] X. Hu, N. Murgovski, L. Johannesson, B. Egardt, Optimal dimensioning and power management of a fuel cell/battery hybrid bus via convex programming, IEEE/ASME Transactions on Mechatronics 20 (1) (2015) 457 – 468.

[19] S. Ahmadi, S. Bathaee, A. H. Hosseinpour, Improving fuel economy and performance of a fuel-cell hybrid electric vehicle (fuel-cell, battery, and ultra-capacitor) using optimized energy management strategy, Energy Conversion and Management 160 (2018) 74 – 84.

[20] X. Han, F. Li, T. Zhang, T. Zhang, K. Song, Economic energy management strategy design and simulation for a dual-stack fuel cell electric vehicle, International Journal of Hydrogen Energy 42 (16) (2017) 11584 – 11595.

[21] F. Martel, S. Kelouwani, Y. Dube, K. Agbossou, Optimal economy-based battery degradation management dynamics for fuel-cell plug-in hybrid electric vehicles, Journal of Power Sources 274 (2015) 367 – 381.

[22] K. Song, F. Li, X. Hu, L. He, W. Niu, S. Lu, T. Zhang, Multi-mode energy management strategy for fuel cell electric vehicles based on driving pattern identification using learning vector quantization neural network algorithm, Journal of Power Sources 389 (2018) 230 – 239.

[23] R. A. Fernandez, S. C. Caraballo, F. B. Cilleruelo, J. A. Lozano, Fuel optimization strategy for hydrogen fuel cell range extender vehicles applying genetic algorithms, Renewable and Sustainable Energy Reviews 81 (2018) 655 – 668.

[24] C. Geng, X. Jin, X. Zhang, Simulation research on a novel control strategy for fuel cell extended-range vehicles, International Journal of Hydrogen Energy, Available online.

[25] M. Carignano, R. Costa-Castello, N. Nigro, S. Junco, A novel energy management strategy for fuel-cell/supercapacitor hybrid vehicles, IFAC-PapersOnLine 50 (1) (2017) 10052 – 10057, 20th IFAC World Congress.

[26] X. Hu, L. Johannesson, N. Murgovski, B. Egardt, Longevity-conscious dimensioning and power management of the hybrid energy storage system in a fuel cell hybrid electric bus, Applied Energy 137 (2015) 913 – 924.

[27] Z. W. Wei Yueyuan, L. Yi, A study on the matching and optimization of fchev powertrain, Automotive Engineering 30 (10) (2008) 918 – 922 + 933, (in Chinese).

[28] A. Purvins, M. Sumner, Optimal management of stationary lithium-ion battery system in electricity distribution grids, Journal of Power Sources 242 (2013) 742 – 755.

[29] X. Wu, X. Hu, X. Yin, S. J. Moura, Stochastic optimal energy management of smart home with pev energy storage, IEEE Transactions on Smart Grid 9 (3) (2018) 2065 – 2075.

[30] S. Ebbesen, P. Elbert, L. Guzzella, Battery state-of-health perceptive energy management for hybrid electric vehicles, IEEE Transactions on Vehicular Technology 61 (7) (2012) 2893 – 2900.

[31] L. Johannesson, N. Murgovski, S. Ebbesen, B. Egardt, E. Gelso, J. Hellgren, Including a battery state of health model in the hev component sizing and optimal control problem, IFAC Proceedings Volumes 46 (21) (2013) 398 – 403, 7th IFAC Symposium on Advances in Automotive Control.

[32] N. Murgovski, Cones: Matlab code for convex optimization in electromobility studies (https://research.chalmers.se/en/publication/?id=192858).

[33] S. Boyd, L. Vandenberghe, Convex Optimization, Cambrige, U.K.: Cabridge Univ. Press, 2004.

[34] X. Wu, X. Hu, Y. Teng, S. Qian, R. Cheng, Optimal integration of a hybrid solar-battery power source into smart home nanogrid with plug-in electric vehicle, Journal of Power Sources 363 (2017) 277 – 283.

[35] M. Chediak, The latest bull case for electric cars: The cheapest batteries ever, Tech. rep., Bloomberg New Energy Finance (BNEF) (2017).

[36] N. Zart, Batteries keep on getting cheaper, Tech. rep., Clean Technia (2017).

[37] M. Gaithersburg, U.s. department of energy hydrogen and fuel cells program, Tech. rep., U.S. Department of Energy (2016).

Table 7: Financial analysis of sub-optimal FC system parameters in different drive cycles.

Drive cycles	P_{FC}	C_T	C_e	C_h
	kW	yuan	yuan	yuan
WVUSUB	50	9.48	5.70	3.78
WVUSUB	45	9.17	5.69	3.48
WVUSUB	44.81 (optimal)	9.15	5.69	3.46
CSHVR	50	8.63	4.80	3.83
CSHVR	45	8.29	4.80	3.49
CSHVR	40	7.96	4.79	3.17
CSHVR	36.59 (optimal)	7.73	4.79	2.94
WVUCITY	50	5.32	2.63	2.69
WVUCITY	45	5.06	2.62	2.44
WVUCITY	40	4.80	2.62	2.18
WVUCITY	35	4.54	2.62	1.92
WVUCITY	30.07 (optimal)	4.28	2.61	1.67
CBDTRUCK	50	3.11	1.59	1.52
CBDTRUCK	45	2.96	1.59	1.37
CBDTRUCK	40	2.80	1.58	1.22
CBDTRUCK	35	2.64	1.58	1.06
CBDTRUCK	30	2.49	1.58	0.91
CBDTRUCK	25	2.33	1.57	0.76
CBDTRUCK	21.62 (optimal)	2.23	1.57	0.66

Table 8: Costs for concatenated CSHVR drive cycles based on different prices of hydrogen.

cycles	L_a	c_h	C_T	C_e	C_h
	km	yuan/kg	yuan	yuan	yuan
1*CSHVR	10.8	40	7.73	4.79	2.94
2*CSHVR	21.6	40	15.46	9.57	5.89
3*CSHVR	32.4	40	23.19	14.36	8.83
4*CSHVR	43.2	40	30.92	19.15	11.77
5*CSHVR	54.0	40	39.51	20.18	19.33
6*CSHVR	64.8	40	49.69	20.18	28.51
7*CSHVR	75.6	40	58.19	20.18	38.01
8*CSHVR	86.4	40	67.83	20.18	47.65
1*CSHVR	10.8	15	3.74	0	3.74
2*CSHVR	21.6	15	7.48	0	7.48
3*CSHVR	32.4	15	11.21	0	11.21
4*CSHVR	43.2	15	14.95	0	14.95
5*CSHVR	54.0	15	18.68	0	18.68
6*CSHVR	64.8	15	22.42	0	22.42
7*CSHVR	75.6	15	26.15	0	26.15
8*CSHVR	86.4	15	29.89	0	29.89

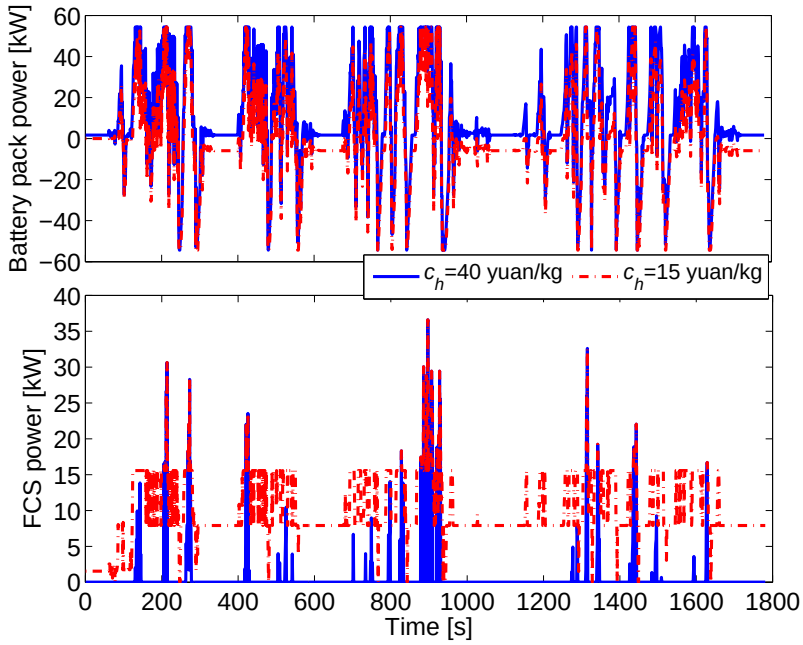

(a) Single CSHVR drive cycle.

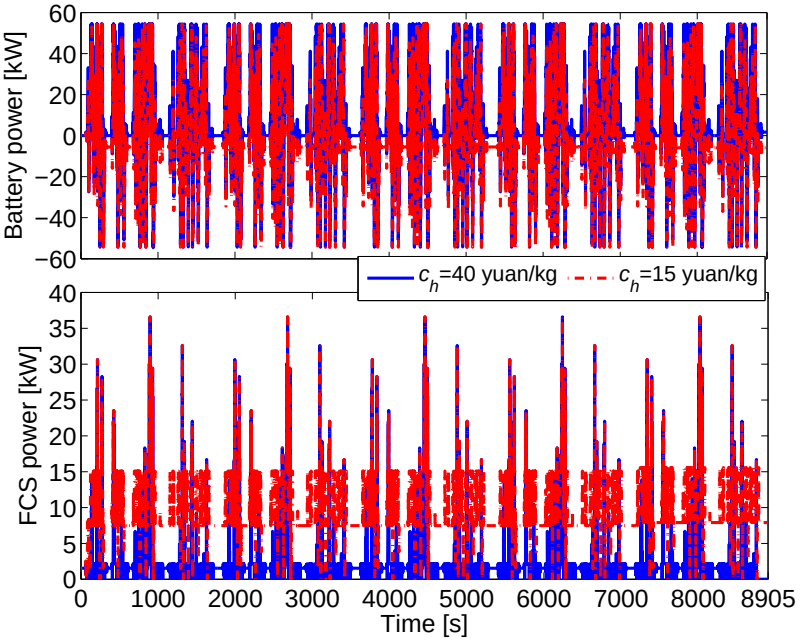

(b) 5 CSHVR drive cycles

Figure 5: Power distribution based on different numbers of CSHVR drive cycles.

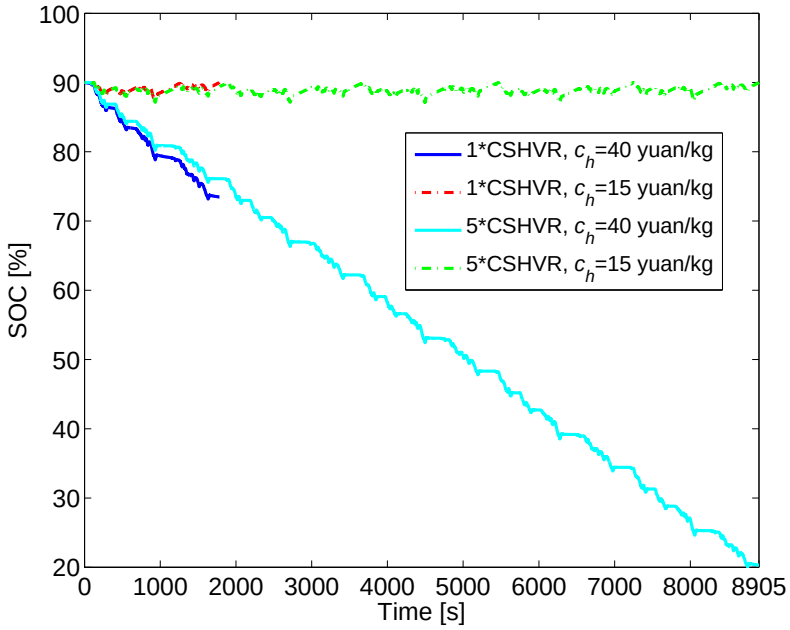

Figure 6: Battery SOC.

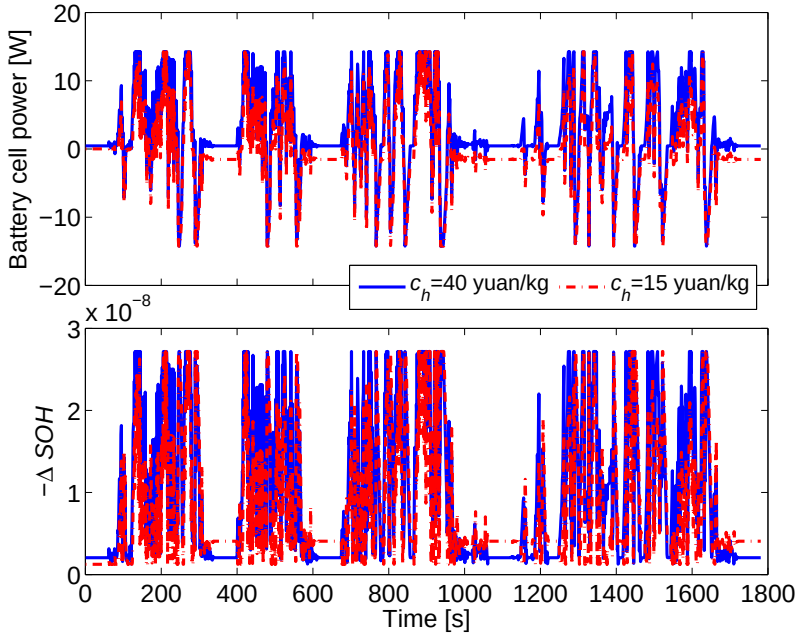

(a) Single CSHVR drive cycle.

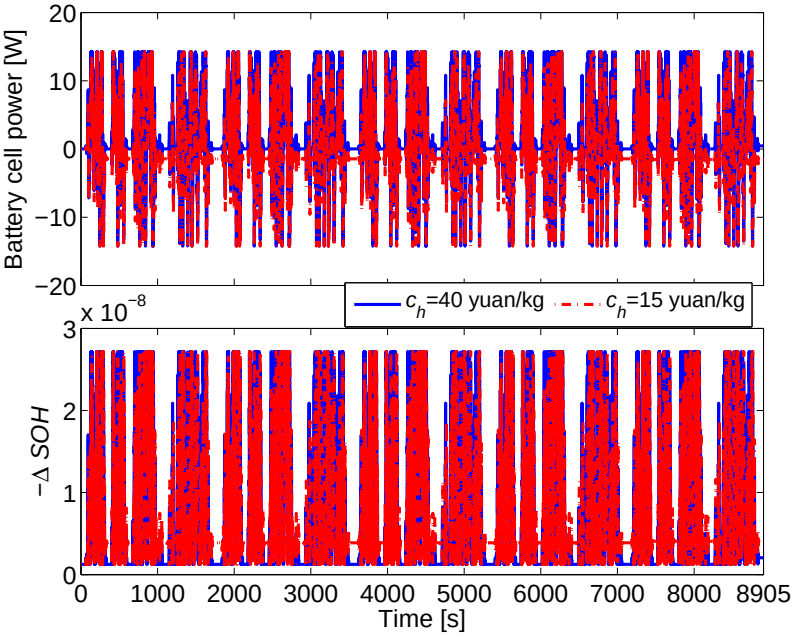

(b) 5 CSHVR drive cycles

Figure 7: Battery cell power and SOH degradation.